Two step processes in pion single charge exchange on ^{2}H at $T_{\pi^+} = 239$ MeV

N. K. Gregory,[5] D. Androić,[9] G. Backenstoss,[1] D. Bosnar,[9] H. Breuer,[4] H. Döbbeling,[8] T. Dooling,[7] M. Furić,[9] P. A. M. Gram,[3] A. Hoffart,[2,8] C. H. Q. Ingram,[8] A. Klein,[7] K. Koch,[8] J. Köhler,[1] B. Kotliński,[8] M. Kroedel,[1] G. Kyle,[6] A. Lehmann,[1,8] A. O. Mateos,[5] K. Michaelian,[8] T. Petković,[9] M. Planinić,[9] R. P. Redwine,[5] D. Rowntree,[5] U. Sennhauser,[8] N. Šimičević,[5] R. Trezeciak,[2] H. Ullrich,[2] M. Wang,[6] M. H. Wang,[6] H. J. Weyer,[1,8] M. Wildi,[1] and K. E. Wilson[5]

(LADS Collaboration)

[1]*University of Basel, CH-4056 Basel, Switzerland*
[2]*University of Karlsruhe, D-76128 Karlsruhe, Germany*
[3]*LAMPF, Los Alamos, New Mexico 87545*
[4]*University of Maryland, College Park, Maryland 20742*
[5]*Massachusetts Institute of Technology, Cambridge, Massachusetts 02139*
[6]*New Mexico State University, Las Cruces, New Mexico 88003*
[7]*Old Dominion University, Norfolk, Virginia 23529*
[8]*Paul Scherrer Institute, CH-5232 Villigen PSI, Switzerland*
[9]*University of Zagreb, HR-10000 Zagreb, Croatia*

(Received 9 June 1998)

Results from a measurement of the reaction $^2\mathrm{H}(\pi^+,pp)\pi^\circ$ at $T_{\pi^+} = 239$ MeV are presented. Because two protons were detected, the measurement was sensitive to events which involved both nucleons in a substantial way. Differential distributions are compared to the predictions of simple models. An integrated cross section for SCX (single charge exchange), with the emission of two protons each with kinetic energy >25 MeV, is presented. [S0556-2813(98)06112-3]

PACS number(s): 25.80.Ls, 25.10.+s, 25.80.Gn

I. INTRODUCTION

The πN interaction is one of the most fundamental reactions in nuclear and particle physics and has been extensively studied. The characteristics of this reaction are thus relatively well known. The effects of adding a second nucleon to the interaction are currently of considerable interest. Efforts have focused on pion absorption and double charge exchange (DCX) on nuclei, for which at least two nucleons must interact with the pion. Another possibility for examining the three-body processes is by looking at single charge exchange (SCX) reactions for kinematics in which both nucleons participate substantially in the reaction. The simplest such process to examine experimentally is SCX on the deuteron, i.e., $\pi^+ d \rightarrow \pi^\circ pp$.

Pion single charge exchange reactions on ^{2}H have usually been measured by detecting the two photons from the decay of the outgoing π° [1–4]. Only one previous work measured the charge exchange reaction on ^{2}H by performing a kinematically complete experiment [5] in which the two outgoing protons were detected. This experiment, however, measured only in the reaction plane and also suffered from small solid angle coverage. The results reported here are from a large-solid-angle study of $\pi^+ d \rightarrow \pi^\circ pp$ in which the energies and angles of the outgoing protons were measured with sufficient precision to determine the identity and momentum of the π°. Because of the detection threshold on the energy of each proton, the portion of the SCX reaction in which both nucleons participated was emphasized.

The experiment was performed in the πM1 channel at the Paul Scherrer Institute [6,7] using the Large Acceptance Detector System (LADS). LADS was constructed to study multi-nucleon pion absorption in the region of the $\Delta(1232)$ resonance. In the process of analyzing the absorption data, it became clear that other reactions could be studied as well. The characteristics important for studying any multi-body final state in the medium-energy regime (large solid angle coverage and low energy thresholds for protons) also make LADS a suitable detector for studying SCX where more than one nucleon is involved. The triggers used to collect the data did not distinguish events with neutral pions and so the SCX data presented here were collected simultaneously with the absorption data.

II. EXPERIMENTAL APPARATUS

The LADS detector was built to cover a solid angle of very nearly 4π steradians [8]. A schematic of the LADS detector is shown in Fig. 1. The detector consisted of a 28-sector barrel closed with 14-sector endcaps. To obtain accurate trajectory information for charged particles, the detector had two cylindrical coaxial multiwire proportional chambers (MWPCs). The scintillator portion of the detector was arranged into ΔE-E-E telescopes which provided particle identification (PID) and timing and energy information for the reaction products. The detector had a proton kinetic energy threshold of ~ 20 MeV, a kinetic energy resolution for protons of 3–5 % FWHM, a vertex resolution of ~ 1.0 mm, and an angular resolution of $\sim 1^\circ$. The target was a 25.7 cm$\times$4 cm diameter carbon fiber/epoxy cylinder containing deuterium at a pressure of 95 bar.

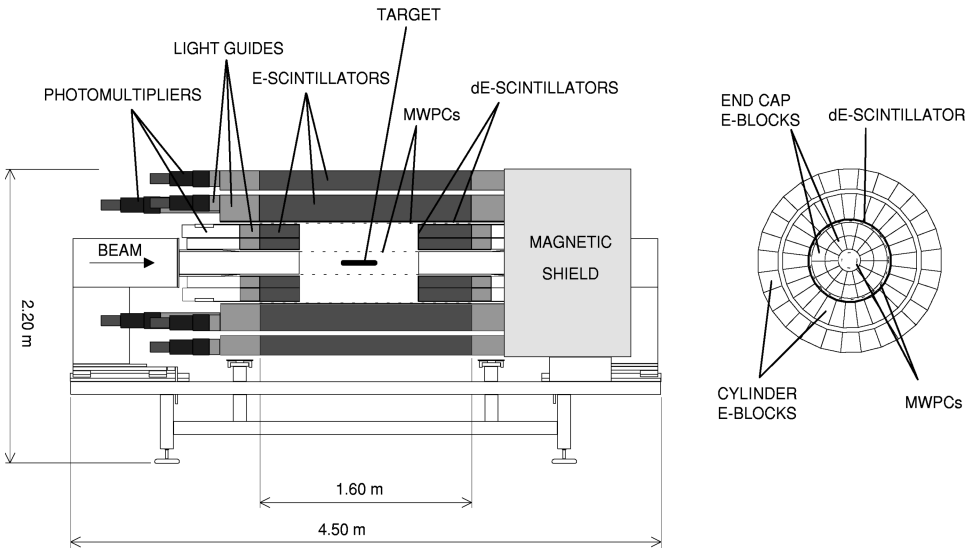

FIG. 1. Schematic of the LADS detector. From Ref. [8].

III. DATA ANALYSIS

The solid angle coverage of the LADS detector, combined with its good energy and angular resolution and relatively low proton energy detection threshold, allowed the examination of different final-state event types. In this analysis, the events of interest were first separated from other events recorded. Contributions from backgrounds were subtracted after being determined by processing the data from empty targets with the same isolation cuts described below. The beam normalization was determined, as was the acceptance of the detector. Acceptance determination involved simulation of different specific reactions and is described in Sec. IV.

A. Event identification

The first step in event identification involved requiring that trajectory information was available from the MWPCs. The vertex could be determined by the intersection of the tracks of two charged particles or taken to be the intersection of a single track and the beam axis. Thus each charged particle had to have at least one MWPC hit associated with it, and at least one charged particle had to have hits in both MWPCs. A cut was applied along the z-position (the beam axis) of the vertex to ensure that the event originated in the ^{2}H.

After isolating events from the target region, SCX events were separated from the other events. The reaction channels could be determined by the types of particles in the final state. This analysis required that an event produced two and only two charged particles in the detector, and that they be protons. Charged particles were identified using conventional $E-dE/dx$ and $E-TOF$ particle identification (PID) techniques. Neutral particles, usually photons from π° decay, were ignored in the analysis.

After the PID cuts, most of the charged pion events were removed, but there was still some contamination from other channels, such as pion absorption. There also were pions that were misidentified as protons. Both forms of contamination were then removed, as described below, to obtain clean SCX events. To simplify the analysis, a minimum kinetic energy of 25 MeV at the event vertex was required for all protons.

The contamination from $\pi d \rightarrow pp$ absorption events was removed in two ways. It was required that none of the events contained back-to-back protons in the $\pi^+ - d$ c.m. frame, as almost all of the back-to-back events were absorption events. This cut removed only $\sim$0.3% of the interesting SCX events. Also, a limit on the sum of the kinetic energies of the detected particles was applied to remove pion absorption events which escaped the first cut.

The misidentified charged pions were removed in two ways. One method applied a loose cut on the $E-TOF$ spectra (independent of the PID procedure). The other method used the invariant missing mass calculated from the two-proton kinematics. There is a prominent peak in the missing mass spectrum at $\sim$135 MeV, the mass of the pion (see Fig. 2), which corresponds to SCX. Events which had an invari-

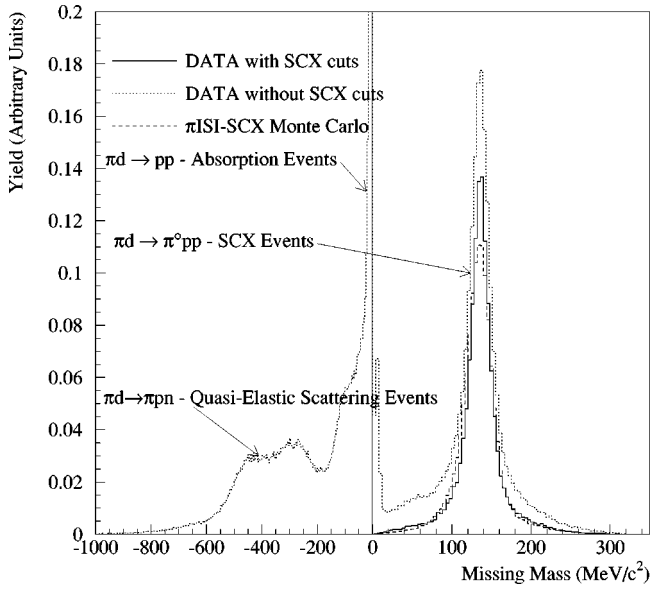

FIG. 2. Calculated invariant missing mass of the proton-proton system. The double peak at 0 is an artifact of the calculation. Note the change in horizontal scale at 0. The Monte Carlo simulation is described in Sec. IV A.

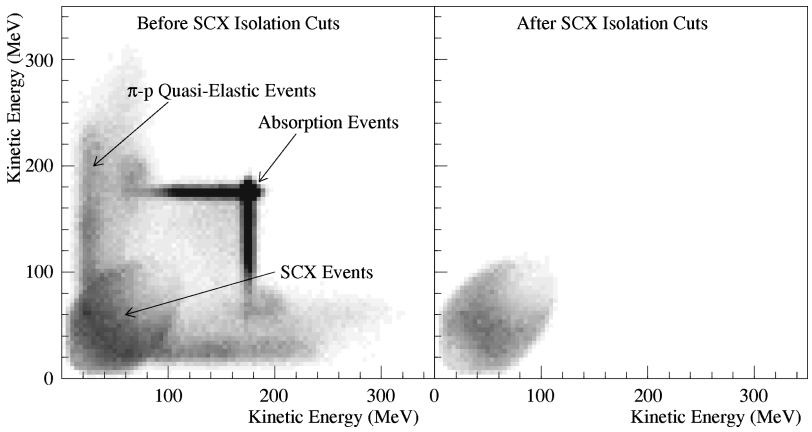

FIG. 3. In the $\pi^+ - d$ c.m. frame, the kinetic energy of ''proton'' 1 is plotted against the kinetic energy of ''proton'' 2. The features in the plots are described in the text.

ant missing mass greater than zero were accepted in our analysis.

The effects of the SCX isolating cuts can be seen in Figs. 3 and 4. In Fig. 3, the kinetic energy of ''proton'' 1 vs the kinetic energy of ''proton'' 2 in the $\pi^+ - d$ c.m. frame are plotted. The left plot shows the data after the target cut and PID. That is, both particles were determined by PID to be protons and the vertex of the event was within the target region. The region in the upper right is populated by $\pi d \rightarrow pp$ absorption events; the horizontal and vertical bands are from absorption events with protons which reacted in the plastic scintillator or passed through the detector. The ellipsoidal locus in the lower left is the region of the SCX events and the ''wings'' which follow the axes correspond to $\pi d \rightarrow \pi pn$ quasielastic scattering events with a misidentified pion. The plot on the right shows what remains after application of the SCX isolation cuts (no back-to-back, positive invariant mass, total kinetic energy, and loose $E - TOF$) and of the 25 MeV proton kinetic energy threshold.

Figure 4 shows a plot of the summed kinetic energy of the event vs the square of the invariant missing mass of the event assuming that both charged particles were protons. The plot on the left shows the data after target and PID cuts. The dark structure on the right contains $\pi^+ - d$ absorption events and the dark structure in the upper left contains SCX events. The gray diagonal band across the plot corresponds to events associated with $\pi^+ - p$ quasielastic scattering. This is a result of the misidentified pions. The plot on the right has all the SCX isolation cuts applied except the invariant mass cut and the total kinetic energy cut. The lines indicated show the position of the invariant mass cut and the total kinetic energy cut. The dot-dashed line is the position of the pion mass. It is seen from the figures that the SCX events were cleanly separated from the other event types.

B. Normalization

To evaluate the cross section, the number of pions incident on the target cell and the number of target scatterers had to be determined. The number of pions reported by the beam defining scintillator [8] was corrected for muon contamination, pion decay, and pions missing the target. The pressure of the target gas of 95 bar was high enough to cause significant deviation from ideal gas behavior. The correction factor to calculate the number of scatterers in the target cell was determined using Ref. [9]. Finally, a correction for the prescaling of event types [8] was applied.

IV. RESULTS

Because of the large solid angle of LADS, many quantities could be investigated. These included various differen-

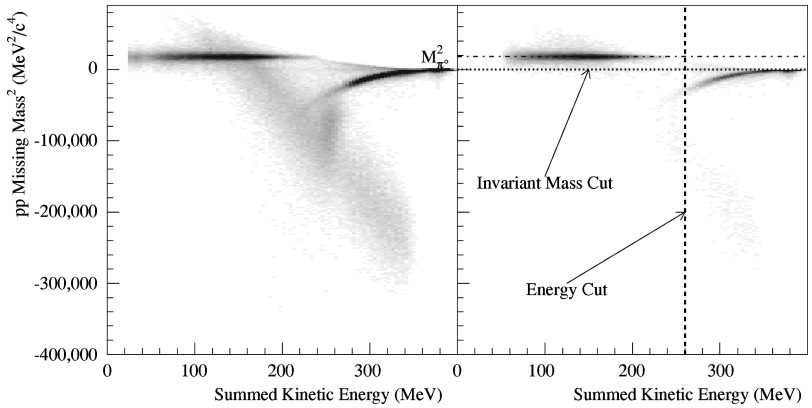

FIG. 4. The sum of the kinetic energies of the detected protons plotted against the square of the proton-proton invariant missing mass. The features in the plots are described in the text.

tial quantities as well as the integrated experimental cross section. Before this could be done, the response of the detector had to be understood so the effects of detector acceptance could be taken into account.

A. Simulations

A Monte Carlo simulation was used to model the detector response and to extrapolate the reaction in question over the unmeasured kinematic regions, in particular below the 25 MeV threshold. The simulation was based on GEANT [10] and designed to use the 4-vectors for protons and pions from different event generators. The code contained the geometry of the scintillator portion of LADS as well as a simulation of the MWPCs. The simulation produced data files that were similar to those produced by the data acquisition system. The simulated data were then processed through the same analysis procedure as the experimental data to determine the detector acceptance. This allowed us to correct for proton reaction losses in the plastic scintillator, for MWPC inefficiencies, and for geometrical acceptances.

Several event generators were written. In the simplest, the three-body phase space for two protons and a pion was filled uniformly. Also written were generators using π-N and N-N phase shifts [11,12] to simulate two-body interactions. All of the phase shift generators used a ''deuteron'' which was created using the nucleon momentum distribution measured by (e,e') experiments [13] to generate a weight for a specific target nucleon momentum.

All of the phase shift generators included the effects of Pauli blocking of the final state protons, represented by the suppression of pions scattered at forward angles. This was accomplished by a weighting function of the relative momentum of the final state protons, which rose from 0 to 1 between 0 and 300 MeV/c and stayed constant above. In addition, for the generators where the SCX occurred first, the polar angle distribution of the neutral pion was weighted by a function which increased from 0 to 1 between 0° and 40° and stayed constant above 40°. The resulting SCX model (see below) is consistent with the data of Park *et al.* [4].

The generators using phase shifts could be separated into two groups based on the number of times the incident pion interacted with the target nucleons. The first group contained generators in which the pion scattered only once. In the spectator model, the incident pion charge exchanged only with the neutron, and the proton in the deuteron was treated as a spectator with a Fermi distributed momentum. The spectator model predictions in subsequent figures are those marked SCX. The SCX–hard-FSI model assumed that the pion charge exchanged with the neutron and that the resultant proton then underwent a ''hard'' collision with the spectator proton. The predictions for the SCX–hard-FSI model are marked in the figures as SCX-HFSI. In the single scattering generators, the spectator nucleon was defined to be on-shell in the deuteron, and the binding energy was taken into account in the pion-nucleon interaction. The weights of the angular distributions were determined by the π-N [11] and N-N [12] phase shifts.

TABLE I. Event generators used in simulating SCX. In this table, σ represents the differential cross section and ρ_N is the measured nucleon momentum distribution in ^{2}H.

Event generator	Monte Carlo weights
Phase space	$\pi^\circ pp$ three-body phase space
SCX	$\rho_N * \sigma_{\pi^+ n \to \pi^\circ p}$
SCX-HFSI	$\rho_N * \sigma_{\pi^+ n \to \pi^\circ p} * \sigma_{pp \to pp}$
πISI-SCX	$\rho_N * \sigma_{\pi^+ p \to \pi^+ p} * \sigma_{\pi^+ n \to \pi^\circ p}$
SCX-πFSI	$\rho_N * \sigma_{\pi^+ n \to \pi^\circ p} * \sigma_{\pi^\circ p \to \pi^\circ p}$

The other group of generators using phase shifts contained the models where the pion interacted twice. One generator used a model in which the pion first elastically scattered off the proton in the deuteron and then charge exchanged with the neutron. The curves from this generator are marked πISI-SCX in the figures. Another generator was based on a double-scattering model which required that the incident pion charge exchanged with the neutron in the deuteron before the neutral pion elastically scattered from the proton in the deuteron. The curves from this generator are marked SCX-πFSI in the figures. The angular weights of the pion scatters were again determined by the π-N phase shifts. The generators and the associated weights are summarized in Table I. A more complete description of the analysis of the data and the models used in the simulation of the data can be found in [14].

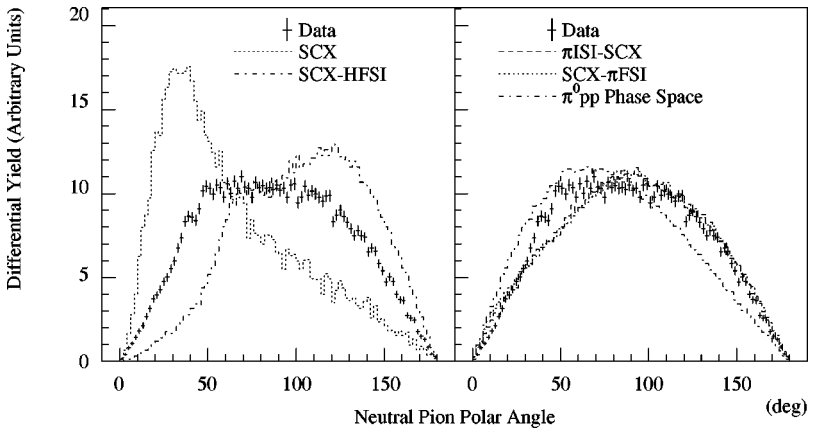

FIG. 5. Polar angle of the reconstructed neutral pion in the laboratory frame with comparison to various models. The error bars are statistical only. The model calculations include the effects of the detector acceptance allowing for direct comparison to the data.

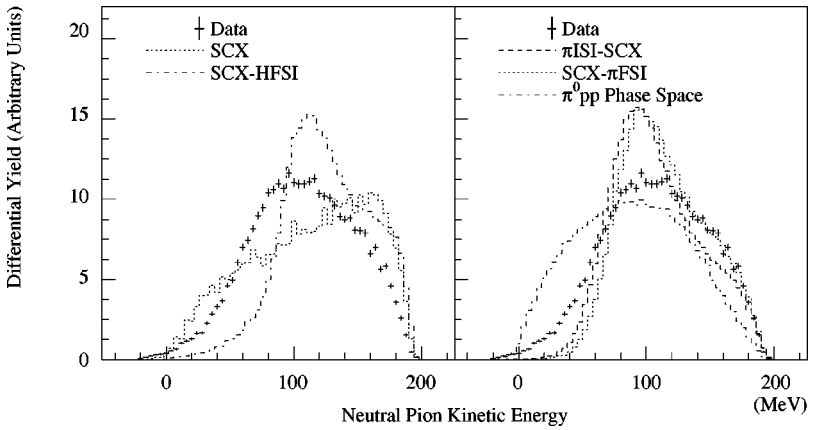

FIG. 6. Kinetic energy of the reconstructed neutral pion in the laboratory frame with comparison to various models. The error bars are statistical only. The model calculations include the effects of the detector acceptance allowing for direct comparison to the data.

B. Acceptance correction and differential distributions

As was stated above, the results of the Monte Carlo simulations were used to determine the acceptance of the detector. The Monte Carlo data were processed in three ways.

LADSOFF0. The energy and angle information from the Monte Carlo generators were taken as their vertex values with no requirement on the minimum energy of the protons.

LADSOFF25. The energy and angle information were taken from the Monte Carlo generators as their vertex values with the requirement that each proton had 25 MeV or more kinetic energy at the vertex.

LADSON25. The results of the Monte Carlo generators were run though the same analysis procedure as were the experimental data with a 25 MeV threshold on the kinetic energy of each proton.

The first step in acceptance correcting the differential spectra was determining which models seem to represent the data. This was done by comparing the LADSON25 distributions with those from the experimental data. Their results are compared to the data in Figs. 5–9. The distributions in these figures were normalized to be equal in area to the experimentally obtained curves.

Figure 5 shows the angular distribution of the reconstructed neutral pions. The left panel shows the data distribution compared with the pion single scattering models, while the right panel is a comparison with the pion double scattering models and three body phase space. For the single scattering simulations, the SCX model is forward-peaked while the SCX-HFSI model is backward-peaked. It is possible to understand the general location of these features by considering the basic cross sections as well as the energy that the pion must lose to bring the protons above threshold. For the spectator model, the cross section is forward-peaked. However, the pion in the FSI model must transfer enough energy to the ''SCX'' proton so that this proton can scatter from the spectator proton and still remain above threshold. To do this, the pion must scatter by a large angle. The fact that the spectator models do not reproduce the data well shows that the pion single-scattering models are not able to describe the process seen by LADS. In contrast, it appears that the pion double scattering models reproduce the data well. Figure 6 shows the kinetic energy distribution of the reconstructed neutral pion. The position of the peak in the data is consistent with the incoming pion losing significant energy at each of two scatters. The spectator model peaks at too high an energy compared with the data. The SCX-HFSI model also peaks at too high an energy and the shape at low energy does not follow the data.

The next three figures present the experimental distributions of the detected protons. Figure 7 shows the angular distribution, and it appears that all models except for the spectator model fit the data reasonably well. Figure 8 pre-

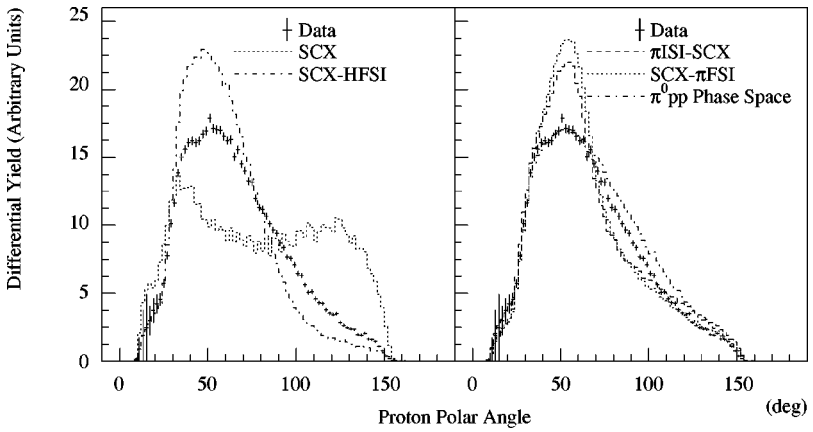

FIG. 7. Polar angle of the detected protons in the laboratory frame with comparison to various models. The error bars are statistical only. The model calculations include the effects of the detector acceptance allowing for direct comparison to the data. Both protons are plotted.

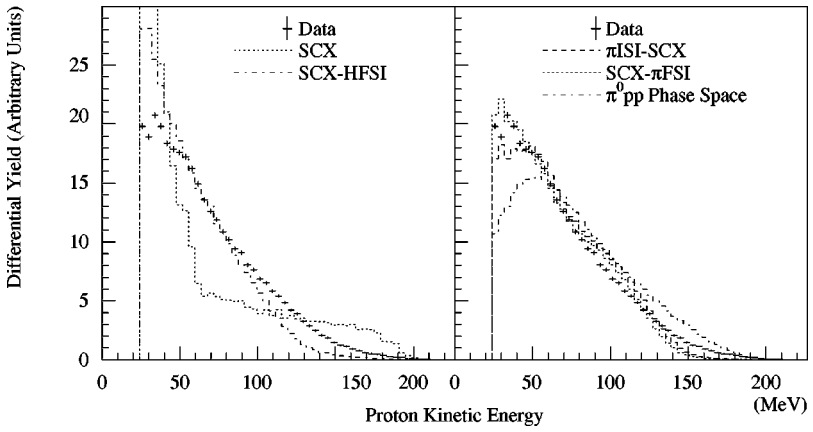

FIG. 8. Kinetic energy of the detected protons in the laboratory frame with comparison to various models. The error bars are statistical only. The model calculations include the effects of the detector acceptance allowing for direct comparison to the data. Both protons are plotted.

sents the kinetic energy distribution of the protons. All of the models except the spectator model fit the data reasonably well though the double scattering models fit the shape the best. Finally, Figure 9 presents the proton-proton opening angle in the laboratory frame. Again the double scattering models fit the data well. The position of the peak in the SCX-HFSI model can be understood by considering the kinematics; i.e., the position of the FSI peak results from the fact that a particle scattering from another particle of equal mass at rest produces two outgoing particles with a 90° opening angle.

From comparing models to all the data, several conclusions can be drawn. First, the models which require that the pion has scattered twice represent the data well. Second, there appears to be little evidence of FSI in the data, which would be indicated by an enhancement at 90° in the p-p opening angle; the output of this generator was not used in the further analysis of the data. Finally, while the data are not perfectly represented by the double scattering models, it does appear that the great majority of the events seen come from a double scattering process.

After having determined which models seem to contribute, the experimental data were fit simultaneously with the processed output of the Monte Carlo generators simulating pion single scattering (SCX) and the pion double scattering models (πISI-SCX and SCX-πFSI) with the normalization of the distributions from each generator as the free parameters. The distributions of the $\pi^{\circ}pp$ phase space model and of the SCX-HFSI model were not used in these fits since they do not represent the data well.

Also, because of the similarity of their distributions, it was not possible to obtain precise separate results for the sizes of the two double scattering processes when fitting all three models simultaneously. Instead, the single scattering model and one of the double scattering models were fit to the data. This was repeated with the other double scattering model with very similar results. The small difference in the results of the fits is included in the uncertainty of the amount of the single scattering contamination (see Sec. IV C). The resulting sum of generators was used to acceptance correct the differential spectra according to the following expression:

$$N_{\mathrm{corr}}(x)=N_{\mathrm{exp}}(x)\,\frac{\Sigma_{i=1}^{N_{\mathrm{models}}}p_i\mathrm{LADSOFF25}_i(x)}{\Sigma_{i=1}^{N_{\mathrm{models}}}p_i\mathrm{LADSON25}_i(x)}, \quad (4.1)$$

where x is the specific histogram channel, i is a specific reaction model, p_i is the fit parameter for the specific model

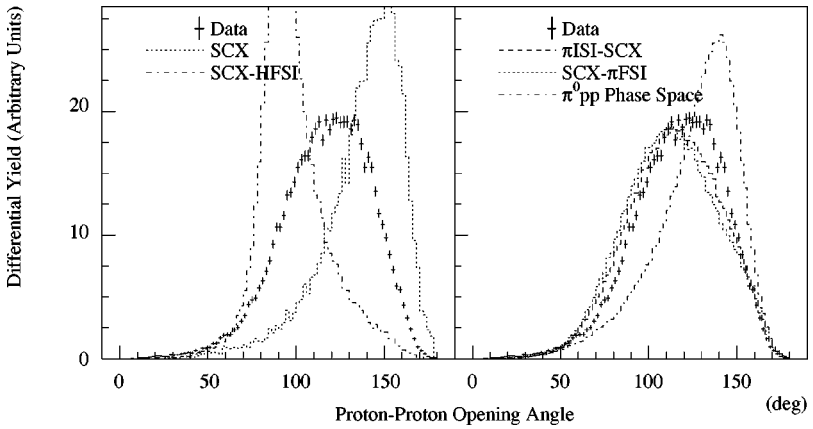

FIG. 9. Proton-proton opening angle in the laboratory frame with comparison to various models. The error bars are statistical only. The model calculations include the effects of the detector acceptance allowing for direct comparison to the data.

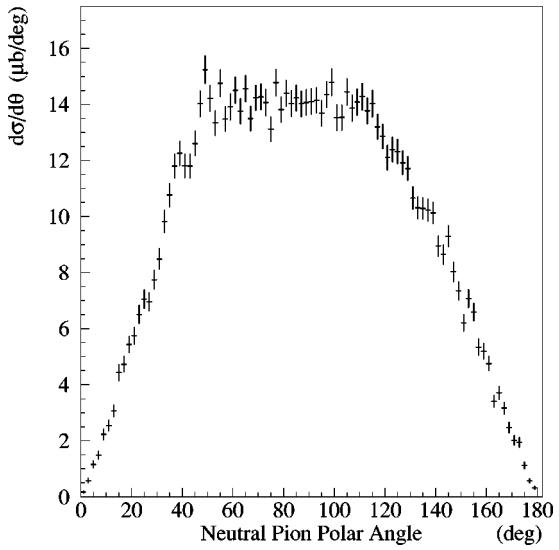

FIG. 10. Polar angle of the reconstructed neutral pion in the laboratory frame. The data have been corrected for the detector acceptance but each proton has a 25 MeV minimum kinetic energy. The error bars are statistical only.

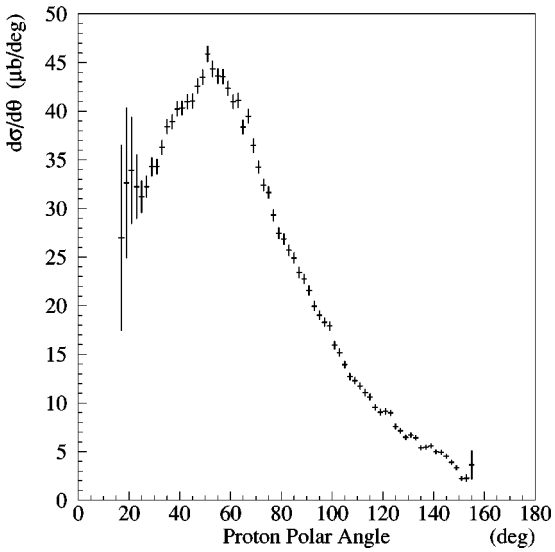

FIG. 12. Polar angle of the detected protons in the laboratory frame. The data have been corrected for the detector acceptance but each proton has a 25 MeV minimum kinetic energy. The error bars are statistical only. Both protons are plotted.

i, LADSON25 and LADSOFF25 are defined above, and $N_{\mathrm{exp}}(x)$ is the number of counts in the particular histogram channel x.

Figures 10–14 show the data corrected for acceptance with a 25 MeV threshold on the kinetic energy of the protons. Figures 10 and 11 are the spectra of the π° and Figs. 12–14 are the spectra of the protons.

In Fig. 15 we compare our data with the doubly differential data of Park *et al.* [15] taken at 263 MeV. It is seen that, as anticipated, the LADS data are mostly in the tails of the quasielastic peak and in the region where one would expect to see multistep events. In the region of the quasielastic peak, the poor agreement with Ref [15] is expected because of the low acceptance of the LADS detector for single-scattering events.

The other kinematically complete measurement of $\pi d \rightarrow pp\pi^{\circ}$ is that of Tacik *et al.* [5]. This experiment was done with small-solid-angle in-plane detectors set at discrete angles. It is not possible from the data acquired to restrict in the analysis the solid angle coverage of our detector to simulate the arrangement in [5] and still be able to make a statistically significant comparison.

C. Integrated cross section

The integrated SCX cross sections measured in this work are summarized in Table II. The total detected yield with two protons of at least 25 MeV, without correction for the detector acceptance, is 1.27 ± 0.05 mb. The SCX cross section for protons above 25 MeV, fully corrected for the detector's

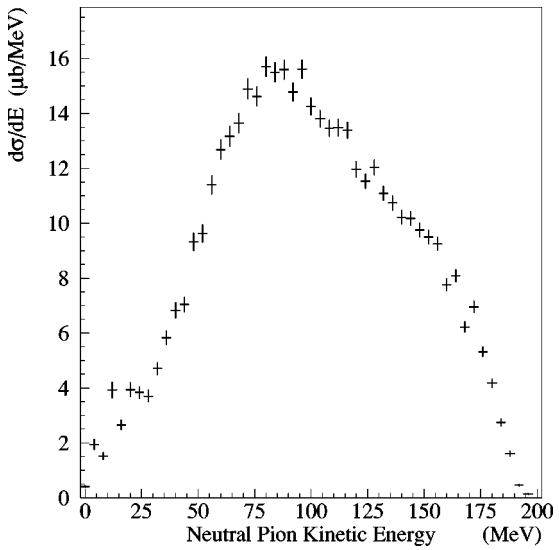

FIG. 11. Kinetic energy of the reconstructed neutral pion in the laboratory frame. The data have been corrected for the detector acceptance but each proton has a 25 MeV minimum kinetic energy. The error bars are statistical only.

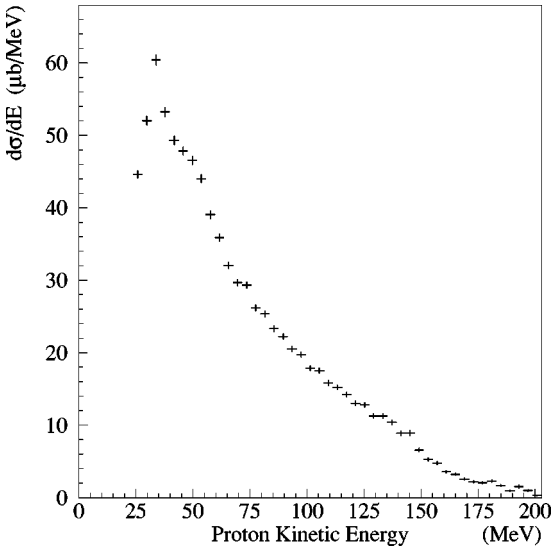

FIG. 13. Kinetic energy of the detected protons in the laboratory frame. The data have been corrected for the detector acceptance but each proton has a 25 MeV minimum kinetic energy. The error bars are statistical only. Both protons are plotted.

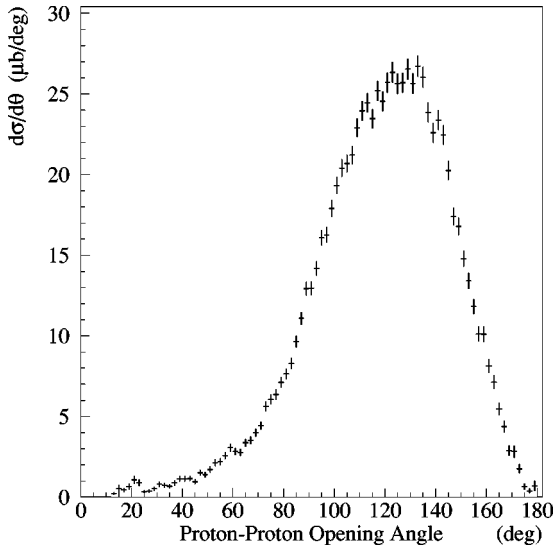

FIG. 14. Proton-proton opening angle, in the laboratory frame. The data have been corrected for the detector acceptance but each proton has a 25 MeV minimum kinetic energy. The error bars are statistical only.

acceptance and inefficiencies, was determined using the fit of the simulations to the data to be 1.7 ± 0.2 mb; the uncertainty here is dominated from those of the fits, including sensitivity to the parameters and sensitivity of the models to the geometry of the LADS detector in the Monte Carlo simulation.

It is also possible to extrapolate the cross section, for that part of SCX from double pion scattering events, down to 0 MeV proton energy using the LADSOFF0 generators. The differential quantities indicate that the majority of the events seen by LADS came from double scattering processes. This was expected as two protons with kinetic energies above 25 MeV must have been detected. One could then determine the acceptance of LADS for the double scattering processes. To do this, an estimate of the mixing ratio of the two processes (πISI-SCX and SCX-πFSI) must be made. If one assumes that the process was dominated by the Δ excitation, and that the scattering was incoherent, then the model which had the pion elastically scattering and then charge exchanging (πISI-SCX) should contribute 9/4 as much as the model which had the pion charge exchanging first (SCX-πFSI). Assuming this ratio, the total acceptance for the LADS detector for events of the double scattering type was determined to be 0.36 ± 0.04, where the uncertainty is an estimate from studies investigating the sensitivity of the acceptance to the Monte Carlo simulations. Because of the similarity of the two double-scattering models in the simulations, the acceptance for double scattering events is in fact not sensitive to the exact ratio of πISI-SCX to SCX-πFSI.

With the data extracted, the background subtracted, and the simulation to correct for the acceptance of the detector processed, we determined an integrated cross section using

$$\sigma_{\mathrm{SCX}} = \frac{\mathrm{Yield}}{\Omega_{\mathrm{LADS}} N_{tgt} N_{\pi}}, \tag{4.2}$$

where Yield is the number of events seen in the experiment, Ω_{LADS} is the acceptance of the LADS detector, N_{tgt} is the number of scattering centers, and N_{π} is the number of incident pions.

There is a nonzero probability of single-scattering events leading to two protons above threshold. The number could be estimated by simultaneously fitting single and double pion scattering models to the data (see also Sec. IV B). From this it was determined that $84 \pm 8\%$ of the yield with both protons above 25 MeV is due to double scattering processes, with the remaining $16 \pm 8\%$ from single scattering.

Subtracting the single scattering cross section contamination and extrapolating the acceptance corrected distributions to 0 MeV proton energy gave the total SCX cross section from double scattering processes to be 3.0 ± 0.5 mb (see Table II). The uncertainty is dominated by the model depen-

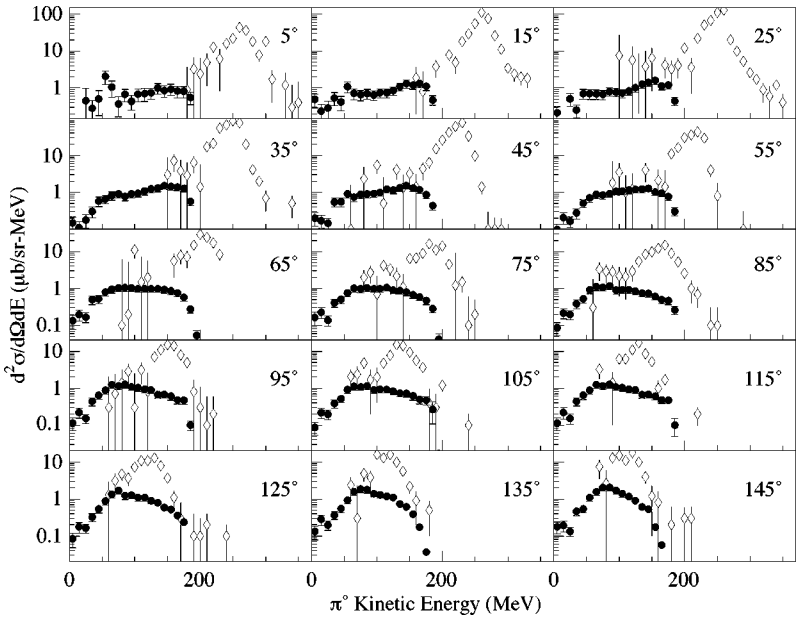

FIG. 15. Doubly-differential cross sections $d^2\sigma/d\Omega dE$. The LADS data are the solid circles, the data from [15] are the diamonds. Note the change of scale in the vertical axis. The 25 MeV threshold on the proton kinetic energy is applied to the data from this work.

TABLE II. The cross section in the top row is the experimental yield. The cross section in the middle row is the integral of the acceptance corrected differential spectra. The cross section in the bottom row is extrapolated to zero energy threshold and is corrected for both acceptance and single scattering contamination.

Cross sections	
Detected cross section with $T_{p_1}, T_{p_2} > 25$ MeV	1.27 ± 0.05 mb
Corrected cross section with $T_{p_1}, T_{p_2} > 25$ MeV	1.7 ± 0.2 mb
Extrapolated cross section for double scattering with $T_{p_1}, T_{p_2} > 0$ MeV	3.0 ± 0.5 mb

dence of the size of the single scattering contribution. Estimates of the total SCX cross section on ^{2}H at this energy were made, based on measurements [1–3] at lower energies and on the data of Ref. [4], and were found to be not far from the cross section of ~ 29 [11] mb on the proton at this energy. The present result thus indicates that double scattering processes account for 10–15 % of the total SCX cross section at 239 MeV.

V. CONCLUSIONS

A unique measurement of pion single charge exchange has been made. The large solid angle of the LADS detector and the measurement method provided access to multiple scattering components of pion interactions with the deuteron. The large solid angle also allowed examination of a number of differential variables. This new data set should provide useful constraints on calculations of multistep pion interactions in light nuclei.

ACKNOWLEDGMENTS

This work was supported in part by the German Bundesministerium für Forschung und Technologie, the German Internationales Büro der Kernforschungsanlage Jülich, the Swiss National Science Foundation, the U.S. Department of Energy, and the U.S. National Science Foundation.

[1] K. C. Rogers and L. M. Lederman, Phys. Rev. **105**, 247 (1957).
[2] E. G. Pewitt, T. H. Fields, G. B. Yodh, J. G. Fetkovich, and M. Derrick, Phys. Rev. **131**, 1826 (1963).
[3] J. H. Norem, Nucl. Phys. **B33**, 512 (1971).
[4] H. T. Park, J. L. Matthews, S. F. Pate, J. F. Amann, C. L. Morris, R. M. Whitton, E. R. Kinney, C. Mertz, and J. Redmon, Phys. Rev. C **51**, R1613 (1995).
[5] R. Tacik, E. T. Boschitz, W. Gyles, C. R. Ottermann, M. Wessler, U. Wiedner, H. Garcilazo, and R. R. Johnson, Phys. Rev. C **42**, 1846 (1990).
[6] J. P. Albanese *et al.*, Nucl. Instrum. Methods **158**, 363 (1979).
[7] R. Balsiger *et al.*, Nucl. Instrum. Methods **157**, 247 (1978).
[8] T. Alteholz *et al.*, Nucl. Instrum. Methods Phys. Res. A **373**, 374 (1996).
[9] L'Air liquide (Firm), *Encyclopedie des Gaz* (Elsevier, Amsterdam and New York, 1976).
[10] GEANT Detector Description and Simulation Tool, *CERN Program Library Long Writeup W5013*, CERN, Geneva, 1993.
[11] J. B. Walter and G. A. Rebka, *SCATPI*, Technical Report LA-7731-MS, Los Alamos Scientific Library, 1979.
[12] R. A. Arndt, J. M. Ford, and L. D. Roper, Phys. Rev. D **32**, 1085 (1985). The code used is SAID.
[13] M. Bernheim, A. Bussière, J. Mougey, D. Royer, D. Tarnowski, S. Turck-Chieze, S. Frullani, G. P. Capitani, E. De Sanctis, and E. Jans, Nucl. Phys. **A365**, 349 (1981).
[14] N. K. Gregory, M.S. thesis, Massachusetts Institute of Technology, 1995.
[15] H. T. Park, Ph.D thesis, Massachusetts Institute of Technology, 1995.